PHYSICAL REVIEW B **91**, 241404(R) (2015)

Floquet interface states in illuminated three-dimensional topological insulators

H. L. Calvo,[1] L. E. F. Foa Torres,[1] P. M. Perez-Piskunow,[1] C. A. Balseiro,[2,3] and Gonzalo Usaj[2,3]
[1]*Instituto de Física Enrique Gaviola (CONICET) and FaMAF, Universidad Nacional de Córdoba, Córdoba, Argentina*
[2]*Centro Atómico Bariloche and Instituto Balseiro, Comisión Nacional de Energía Atómica, 8400 Bariloche, Argentina*
[3]*Consejo Nacional de Investigaciones Científicas y Técnicas (CONICET), Argentina*
(Received 13 February 2015; revised manuscript received 29 May 2015; published 15 June 2015)

Recent experiments showed that the surface of a three-dimensional topological insulator develops gaps in the Floquet-Bloch band spectrum when illuminated with a circularly polarized laser. These Floquet-Bloch bands are characterized by nontrivial Chern numbers which only depend on the helicity of the polarization of the radiation field. Here we propose a setup consisting of a pair of counterrotating lasers, and show that one-dimensional chiral states emerge at the interface between the two lasers. These interface states turn out to be spin polarized and may trigger interesting applications in the field of optoelectronics and spintronics.

DOI: 10.1103/PhysRevB.91.241404 PACS number(s): 73.20.At, 72.25.−b, 73.43.−f, 78.67.−n

Introduction. Amid the excitement sparked by graphene [1,2] and its record properties [3], the discovery of topological insulators (TIs) [4,5] developed with surprising speed. Indeed, TIs were predicted two years earlier in graphene [6], but the necessary spin-orbit interactions were too weak for this to be observed and a different playground was needed to realize them [7]. Most TIs are three-dimensional (3D) materials as are usual solids, but with a special property: They have a bulk band gap while keeping states that propagate with unprecedented robustness at the periphery of the sample [8,9]. These peculiar states hold great promise for quantum computation [10] but at the same time open up a major challenge: Controlling them is particularly demanding for 3D TIs.

Encompassing the rapid progress in graphene photonics [11] and optoelectronics [12,13], theoretical studies predicted the formation of laser-induced band gaps [14] in graphene when properly tuning the laser polarization, frequency, and intensity [15–18]. More recently, these gaps were unveiled at the surface of a TI through angle-resolved photoemission spectroscopy (ARPES) [19]. This triggered great expectations for achieving laser-assisted control not only in the form of an on-off switch for the available states, but also because theoretically nontrivial topological states [14,20,21] can be induced on a diversity of materials [22–26], and also in cold matter physics [27,28]. Exciting questions arise about the nature of these novel states [29–44], the possibilities for manipulating them [31], the associated topological invariants [32–36], their statistical properties [37–40], and their two-terminal [41,42] and multiterminal (Hall) responses [43,44]. Still, an experimental realization of the Floquet chiral edge states is missing. Most studies considered two-dimensional (2D) systems, except for Refs. [45,46], where the target was a 3D semiconductor.

Here, we show that, besides opening a band gap as in Ref. [19], illuminating a 3D TI with a suitable set of lasers can confine the surface states into one-dimensional states which also bear a topological origin. The proposed setup is represented in Fig. 1: two lasers with opposite circular polarization incident perpendicularly to a face of a 3D TI. This can be devised through, e.g., a single laser beam split into two with opposite helicity. The interface between the lasers is assumed to be shorter than the thermalization length so that the occupations are determined by the (larger) regions without radiation. As we will see below, this modification of the experimental setup in Ref. [19] introduces Floquet states propagating along the boundary where the polarization changes. Our results follow from simulations of the Floquet spectra based on low-energy models, which are further supported by (i) a calculation of the topological invariants and (ii) explicit calculations for a driven 3D lattice model. Interestingly, we show that the resulting Floquet boundary states, which arise from a topological transition between the illuminated regions, carry spin-polarized currents.

Illuminated TIs and Floquet theory. We consider a low-energy Hamiltonian describing the surface of a TI. Assuming the $(00\bar{1})$ direction [47] and linear order in $\boldsymbol{k}$, the effective surface Hamiltonian reads $H_0 = \hbar v(k_y\sigma_x - k_x\sigma_y)$, where σ_x and σ_y are Pauli matrices describing the spin degree of freedom. The time-dependent field is included through the Peierls substitution $\boldsymbol{k} \to \boldsymbol{k} + e\boldsymbol{A}(t)/\hbar c$, with $\boldsymbol{A}(t)$ the laser's vector potential. In the regions dominated by one of the two lasers, i.e., $|x| \gg x_0$, with x_0 the characteristic length of the lasers' interface (see Fig. 1), we choose a circularly polarized field $\boldsymbol{A}_\tau(t) = A_0[\cos(\tau\Omega t + \varphi)\boldsymbol{e}_x + \sin(\tau\Omega t + \varphi)\boldsymbol{e}_y]$, where $\tau = \pm 1$ sets the direction of rotation and φ determines its orientation (measured from the x axis) at $t = 0$ and, as shown later on, it becomes relevant at the interface's region $x \sim 0$. The time-dependent Hamiltonian thus reads

$$H_\tau(t) = H_0 + \gamma\sin(\tau\Omega t + \varphi)\sigma_x - \gamma\cos(\tau\Omega t + \varphi)\sigma_y, \quad (1)$$

where $\gamma = veA_0/c$ characterizes the strength of the perturbation. A suitable description of the dc spectrum and the topological properties of the system can be achieved through the Floquet theory. By using Floquet's theorem, we obtain a time-independent Hamiltonian in Floquet space, defined as the direct product $\mathcal{R}\otimes\mathcal{T}$ between the usual Hilbert space $\mathcal{R}$ and the space of time-periodic functions $\mathcal{T}$. This space is spanned by the states $|\Psi_\sigma, m\rangle$, where $\sigma = \{\uparrow, \downarrow\}$ accounts for spin and m is the Fourier index. The Floquet Hamiltonian writes

$$\mathcal{H}_F^\tau(\boldsymbol{k}) = H_0\otimes I + I\otimes N_\Omega + i\gamma\tau\sum_{\beta=\pm}\beta\, e^{-i\beta\tau\varphi}\sigma_{\beta\tau}\otimes\Delta_\beta, \quad (2)$$

where we use $\sigma_\pm = (\sigma_x \pm i\sigma_y)/2$. Such a Hamiltonian can be imagined as a series of replicas (Floquet channels) of H_0, each one defined in a Fourier component of the driving. The static

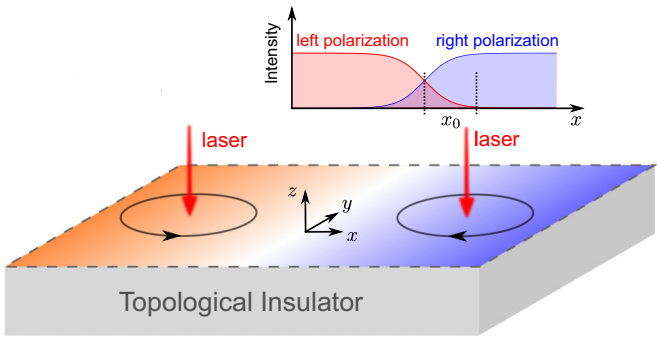

FIG. 1. (Color online) Scheme of the proposed setup where the surface of a 3D TI is illuminated by two circularly polarized lasers with opposite directions of rotation. The y axis defines the interface region between the two lasers. The dashed line in the border indicates that the system extends indefinitely in the x-y plane. Inset: Laser intensities as functions of the x coordinate. At the interface, the two lasers interfere and the total field becomes linearly polarized.

H_0 enters in the diagonal part, together with the contribution $[N_\Omega]_{n,m} = m\hbar\Omega\delta_{n,m}$ from the driving field, and the vector potential couples, through $[\Delta_\beta]_{n,m} = \delta_{m,n-\beta}$, those channels differing in their Fourier indices by $\Delta m = \pm 1$.

For the calculation of the laser-induced band gaps and the associated Chern numbers, it is enough to consider a homogeneous system defined at the TI's surface through Eq. (2). The underlying assumption is that $\hbar\Omega$ is smaller than the bulk gap, such that the states associated with the bulk do not participate in the gap openings. As discussed in Refs. [22,35], these laser-induced gaps are indeed depletions of the time-averaged density of states which result from weighting the Floquet spectrum on the $m = 0$ channel. By assuming low intensities ($\gamma/\hbar\Omega \ll 1$) we restrict ourselves to the main contributions to the band gap openings around $\varepsilon = \hbar\Omega/2$ and at the Dirac point $\varepsilon = 0$, henceforth called the zone boundary (ZB) and the zone center (ZC) gaps, respectively. These two gaps were described in Ref. [48], obtaining $\Delta_1 \approx \gamma$ and $\Delta_0 \approx 2\gamma^2/\hbar\Omega$ for the ZB and ZC gaps, respectively. Notice that a $\pi/2$ rotation along the z direction of the spin coordinate system maps H_0 to the low-energy Hamiltonian describing a single valley in graphene ($H_0 \to \hbar v \boldsymbol{k}\cdot\boldsymbol{\sigma}$). Therefore, apart from a change in the Fermi velocity, the laser-induced gaps show the same dependencies in both systems [14,15,49].

The equivalence between Eq. (2) and the low-energy description for illuminated graphene can be exploited even further: In graphene, the laser-induced gaps are characterized by nontrivial Chern numbers, and the bulk-boundary correspondence leads to Floquet chiral states at the sample edges [22,35,41]. Can similar states appear here? A first problem is simply that the surface of a 3D solid cannot have a boundary. This motivates our proposal of changing the light polarization as in Fig. 1, thereby introducing an effective boundary (much as a domain wall, as discussed in other examples [50–52]) where Floquet chiral states develop—by chiral we mean that the direction of motion is fixed by the helicity of the two lasers.

Starting from Eq. (2), we proceed as in Refs. [35,53]: First, we isolate each crossing where a band gap opens, and then we compute a 2×2 effective Hamiltonian of the form $\mathcal{H}_{\rm eff} = \boldsymbol{h}\cdot\boldsymbol{\sigma}$. The contribution to the Chern number of the lower band can be calculated through the expression [9]

$$C = \frac{1}{4\pi}\int d^2\boldsymbol{k}\,\frac{\boldsymbol{h}}{h^3}\cdot\left(\partial_{k_x}\boldsymbol{h}\times\partial_{k_y}\boldsymbol{h}\right). \tag{3}$$

In the ZB gap region, the band gap opening comes from the crossing between the states $|\Psi_+,0\rangle$ and $|\Psi_-,1\rangle$. Here, $|\Psi_\pm\rangle$ refer to the conduction and valence band solutions of H_0, respectively, and the second index (0 or 1) indicates the Floquet channel. By reducing the Floquet Hamiltonian to these states, we obtain that the contribution to the Chern number is $C_1 = \tau$. In the ZC region there are two processes related to the gap opening. These consist of (i) the renormalization of $|\Psi_\pm,0\rangle$ due to the coupling to the $m = \pm 1$ states, and (ii) the level crossing between $|\Psi_-,1\rangle$ and $|\Psi_+,-1\rangle$, bridged by the $m = 0$ states. A straightforward calculation of these two contributions yields $C_0 = -\tau/2 + 2\tau = 3\tau/2$. While in graphene this half-integer Chern number is compensated by spin and valley degeneracies, in strong TIs, where the surface encloses an odd number of Kramers degenerate Dirac points, a half-integer Chern number results, for example, when exposing the material to a static magnetic field [9,51,54–57].

Interface states in 3D TIs. A natural question relies on the bulk-boundary correspondence in illuminated TIs associated to the nonzero Chern numbers of the Floquet bands. In the present case, since inverting the helicity of the circularly polarized laser changes the sign of the Chern numbers, one expects the generation of chiral states at the boundary between the two regions.

To elucidate this question we proceed by solving the proposed model at the laser's interface. For simplicity in the calculation we assume a sudden change in the laser's direction of rotation by assigning a different τ to each portion of the system [according to Fig. 1, $\tau(x) \equiv -\mathrm{sgn}(x)$]. The resulting differential equation therefore reads

$$\partial_x\boldsymbol{\Psi}(\boldsymbol{r}) = \mathcal{M}_{\tau(x)}\boldsymbol{\Psi}(\boldsymbol{r}), \tag{4}$$

where $\mathcal{M}_\tau = i\sigma_y(\mathcal{H}_F^\tau(k_y\,\boldsymbol{e}_y) - \varepsilon\mathcal{I})/v$ and $\boldsymbol{\Psi}(\boldsymbol{r}) = e^{ik_y y}(\psi_{\uparrow,0},\psi_{\downarrow,0},\psi_{\uparrow,1},\psi_{\downarrow,1})^{\rm T}$ contains the wave-function coefficients $\psi_{\sigma,m}(x)$ for the involved channels [58]. The solutions to the above differential equation follow a standard diagonalization of $\mathcal{M}_\tau$ in the two regions with the appropriate boundary condition [47] and is discussed in detail in the Supplemental Material [59].

In Fig. 2 we show the resulting localized states in both the ZB and ZC gaps in a configuration of $\varphi = \pi/2$, such that at $t = 0$ the vector potentials point parallel to the interface's direction. Our calculations allow one to verify the bulk-boundary correspondence. Indeed, the difference between forward and backward propagating states (relative to the y axis) is always fixed to the calculated difference between the Chern invariants at each side of the interface, yielding $\Delta C_1 = -2$ for the ZB gap and $\Delta C_0 = -3$ for the ZC gap. Other choices in the orientation φ lead to changes in the dispersions of the chiral states but keeping these numbers the same [59]. Although never crossing the gaps, additional states localized at the interface are also present—since they are not chiral, one could expect these states to backscatter when encountering impurities in the sample. In Fig. 2(a) (inset) we show the time-averaged probability density, $\bar{P}(x) = \sum_{m,\sigma}|\psi_{\sigma,m}(x)|^2$, associated with one of the

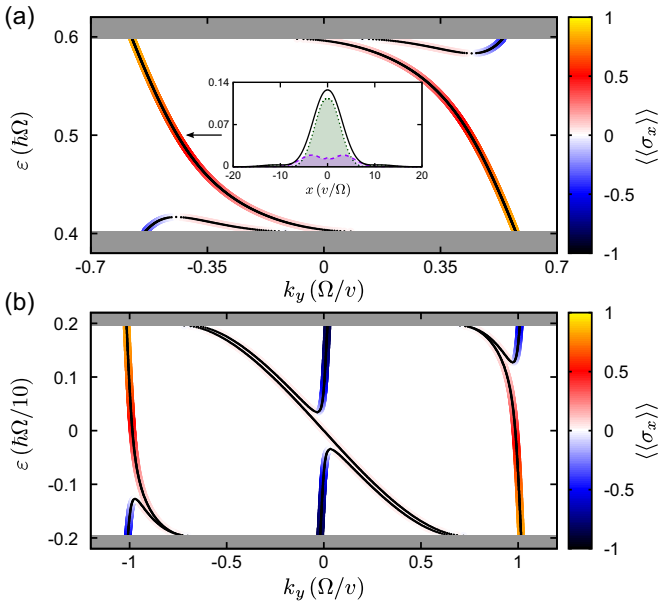

FIG. 2. (Color online) Laser generation of interface states crossing the (a) ZB and (b) ZC gaps. Gray regions indicate extended states zones. The color scale shows the time-averaged spin texture $\langle\langle\sigma_x\rangle\rangle$. Inset: Time-averaged probability density $\bar{P}$ for the state at $\varepsilon = \hbar\Omega/2$ in a solid line (black). The dotted line (green) shows the $m = 0$ component while the dashed line (purple) is for $m = 1$. Here we use $\gamma/\hbar\Omega = 0.2$ and $\varphi = \pi/2$.

two localized states crossing the gap at $\varepsilon = \hbar\Omega/2$ (negative k_y). Here, the decay length depends inversely on the size of the gap and, similarly to illuminated graphene [22,35], it is independent of the microscopic details of the sample. In a more realistic situation where the inversion of the laser helicity is taken gradually over a finite length x_0 (see below), the width of these states shows a dependence also on the latter parameter x_0. It can be seen also that there is a pronounced asymmetry in the contributions from the $m = 0$ and $m = 1$ channels to the overall probability density, which is particular to the relative angle between φ and the direction of the interface. The other state developed at positive k_y shows to have this asymmetry inverted.

Using the solutions of Eq. (4) we calculate the time-averaged spin texture [35] associated with the Floquet boundary states. Owing to the spin-momentum locking present in the TI without radiation, there is a nonvanishing spin component in the Floquet states, $\langle\langle\sigma_x\rangle\rangle = 2\sum_m \int \mathrm{Re}[\psi^*_{\uparrow,m}(x)\psi_{\downarrow,m}(x)]dx$, i.e., the in-plane component perpendicular to the interface's direction. In all cases, $\langle\langle\sigma_x\rangle\rangle$ is proportional to the group velocity, as can be seen in Fig. 2. Since the direction of propagation can be tuned by the lasers, these robust states could be also interesting from the point of view of spin-polarized transport at a desired region of the TI's surface.

Three-dimensional lattice model and local density of states (LDOS). Up to now our analysis is based on an effective 2D model for the surface states of a TI. This poses the question on whether these properties can be reproduced in a model accounting for the insulating bulk bands of a 3D TI. We therefore consider a lattice Hamiltonian which satisfies the four symmetries present in a strong TI [47]. By taking a cubic lattice with parameter a, we obtain a tight-binding description for an isotropic TI [51]. The vector potential $\boldsymbol{A}(\boldsymbol{r},t) = \sum_{\tau=\pm} \boldsymbol{A}_\tau(z,t) f(\tau x)$ enters through a Peierls' substitution as a time-dependent modulation of the hopping matrices coupling nearest neighbor sites. This accounts for (i) a gradual change $f(x) = [1 + \exp(x/x_0)]^{-1}$ of the laser helicity, which produces a φ-oriented, linearly polarized field at the interface region, and (ii) a photon absorption process across the layers of the TI which manifests through a decay in the laser intensity, $A_0(z) = a_0\xi^{-z/z_0}$. In our simulations, ξ and z_0 are adjusted in such a way that the laser becomes negligible at the bottom face of the irradiated sample. The resulting lattice Hamiltonian is derived in the Supplemental Material [59].

In Fig. 3 we show the time-averaged k_y-resolved LDOS (ρ_{k_y}) [22,35] in a geometry [see Fig. 3(a)] where the solid is infinite along the x and y directions, while in the z direction it has $N_z = 9$ layers. A quantitative description is possible by adjusting the model parameters to, e.g., those estimated in Ref. [60], yielding larger values of N_z. In Fig. 3(b) we calculate ρ_{k_y} for the nonilluminated material, where the gapless surface state crossing the bulk gap can be appreciated. Turning on the lasers, we evaluate ρ_{k_y} at different points of the sample. Figure 3(c) shows the sample's bulk region, where there is a clear absence of states within the insulating bulk gap. When moving to the top surface, to a region dominated by only one of the two lasers, Fig. 3(d) reveals the ZB and ZC gaps similar to those observed in Ref. [19]. Finally, once we arrive at the interface region, Fig. 3(e) shows the emergence of chiral states similar to those of Fig. 2. In the ZC region [bottom panels in Fig. 3(f)], we can observe that, due to the small width of the gap, the central state (forward mover) *apparently* crosses it, reflecting the $-\tau/2$ contribution to C_0 from the renormalization of the $m = 0$ states. Similar to Fig. 2(b) there is, however, a small admixture which hybridizes this forward mover state with the degenerate states around $k_y \sim 0$ (backward movers), and the final state crossing the gap shows a negative slope, as required by ΔC_0. In this sense, the difference in the number of states with opposite direction of motion is again bounded to the calculated topological invariants C_0 and C_1 on each side of the interface and does not depend on its specific shape. The details of the wave functions and of the quasienergy dispersion, however, do depend on the angle between the interface and the orientation φ of the linearly polarized vector potential formed at that point [59].

Final remarks. In summary, we found that illuminating the surface of a 3D TI with a pair of counterrotating lasers generates chiral, one-dimensional states confined at the interface region between the lasers. These states locate within the recently measured laser-induced gaps in ARPES [19], for which we believe a small modification of the experimental setup would be enough for its observation. Additionally, these states have a finite time-averaged spin texture subjected to the spin-momentum locking effect of the bare material, making them interesting from the point of view of spin-polarized transport. Our calculations in the low-energy regime are supported by simulations in a 3D lattice model, which accounts for the interface zone. Given the topological character of the Floquet bands, the qualitative properties of these interface states (chirality and spin-momentum locking) remain unaffected by the experimental details of the laser configuration (e.g., fluctuations in their relative phase). Importantly, the existence of the topological states is not bounded to the local

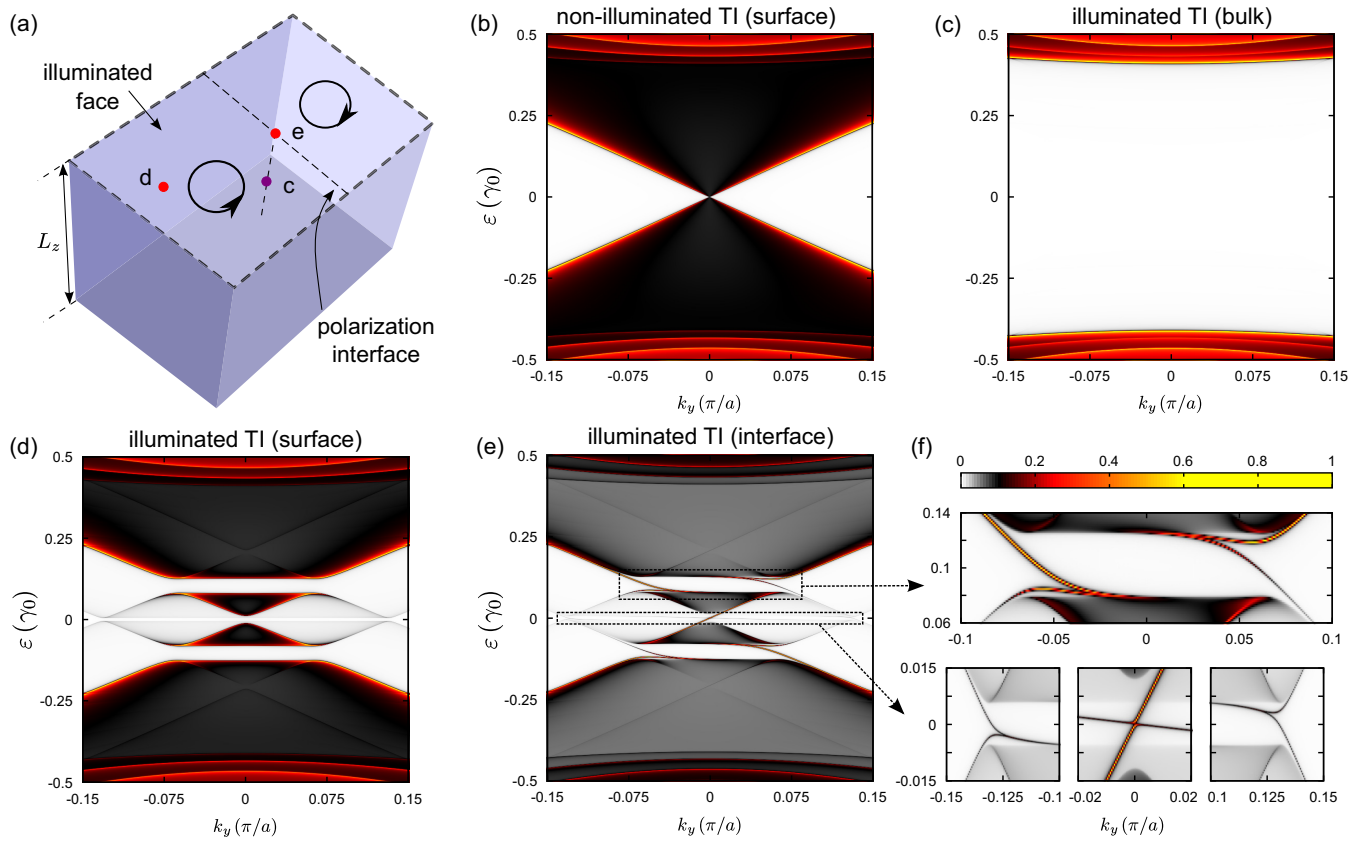

FIG. 3. (Color online) Normalized ρ_{k_y} in an isotropic model for a 3D TI with $L_z = 9a$: (a) Schematics of the considered setup indicating the different points at which ρ_{k_y} is evaluated. (b) At the surface of a static TI. (c) Irradiated sample at the insulator's bulk ($z = 5a$). (d) At the surface, away from the interface's region, here only one of the two lasers dominates. (e) At the surface, across the interface's region. (f) The color scale used in all plots and a closeup of (e) at the ZB (top panel) and the ZC (bottom panels) regions. In all cases, the parameters used for the static Hamiltonian are $m_0 = 0.4$, $m_1 = 0.25$, and $m_2 = 0.5$ [51], and the laser parameters are $\hbar\Omega = 0.2\gamma_0$, $\eta_0 = 2\pi a_0 a/\Phi_0 = 0.1$ [59], $\varphi = \pi/2$, $x_0 = 3a$, $\xi = 0.8$, $z_0 = a$, and include the Floquet channels $m = \{-1,0,1\}$.

recovery of the time-reversal symmetry at the interface [61]. Other choices in the setup including, e.g., the simultaneous irradiation of different faces of the TI, are of great interest and deserve further exploration since one could exploit different spin textures and band curvatures [47,52] to achieve control over the chiral states.

Acknowledgments. We acknowledge financial support from SeCyT-UNC, ANPCyT (PICT Bicentenario 2010-1060, PICT 2013-1045), CONICET (PIP 11220110100832) and SeCTyP-UNCuyo (06/C415), ICTP's associateship program (L.E.F.F.T. and G.U.), the Alexander von Humboldt Foundation (L.E.F.F.T.), and the Simons Foundation (G.U.).

[1] K. S. Novoselov, A. K. Geim, S. V. Morozov, D. Jiang, M. I. Katsnelson, I. V. Grigorieva, S. V. Dubonos, and A. A. Firsov, Two-dimensional gas of massless Dirac fermions in graphene, Nature (London) **438**, 197 (2005).

[2] Y. Zhang, Y.-W. Tan, H. L. Stormer, and P. Kim, Experimental observation of the quantum Hall effect and Berry's phase in graphene, Nature (London) **438**, 201 (2005).

[3] A. K. Geim and K. S. Novoselov, The rise of graphene, Nat. Mater. **6**, 183 (2007).

[4] M. König, S. Wiedmann, C. Brüne, A. Roth, H. Buhmann, L. W. Molenkamp, X.-L. Qi, and S.-C. Zhang, Quantum spin Hall insulator state in HgTe quantum wells, Science **318**, 766 (2007).

[5] D. Hsieh, D. Qian, L. Wray, Y. Xia, Y. S. Hor, R. J. Cava, and M. Z. Hasan, A topological Dirac insulator in a quantum spin Hall phase, Nature (London) **452**, 970 (2008).

[6] C. L. Kane and E. J. Mele, Quantum spin Hall effect in graphene, Phys. Rev. Lett. **95**, 226801 (2005).

[7] B. A. Bernevig, T. L. Hughes, and S.-C. Zhang, Quantum spin Hall effect and topological phase transition in HgTe quantum wells, Science **314**, 1757 (2006).

[8] L. Fu and C. L. Kane, Topological insulators with inversion symmetry, Phys. Rev. B **76**, 045302 (2007).

[9] M. Z. Hasan and C. L. Kane, Colloquium: Topological insulators, Rev. Mod. Phys. **82**, 3045 (2010).

[10] J. E. Moore, The birth of topological insulators, Nature (London) **464**, 194 (2010).

[11] F. Bonaccorso, Z. Sun, T. Hasan, and A. C. Ferrari, Graphene photonics and optoelectronics, Nat. Photonics **4**, 611 (2010).

[12] M. Glazov and S. Ganichev, High frequency electric field induced nonlinear effects in graphene, Phys. Rep. **535**, 101 (2014).

[13] R. R. Hartmann, J. Kono, and M. E. Portnoi, Terahertz science and technology of carbon nanomaterials, Nanotechnology **25**, 322001 (2014).

[14] T. Oka and H. Aoki, Photovoltaic Hall effect in graphene, Phys. Rev. B **79**, 081406 (2009).

[15] H. L. Calvo, H. M. Pastawski, S. Roche, and L. E. F. Foa Torres, Tuning laser-induced band gaps in graphene, Appl. Phys. Lett. **98**, 232103 (2011).

[16] Y. Zhou and M. W. Wu, Optical response of graphene under intense terahertz fields, Phys. Rev. B **83**, 245436 (2011).

[17] S. E. Savelev and A. S. Alexandrov, Massless Dirac fermions in a laser field as a counterpart of graphene superlattices, Phys. Rev. B **84**, 035428 (2011).

[18] E. Suarez Morell and L. E. F. Foa Torres, Radiation effects on the electric properties of bilayer graphene, Phys. Rev. B **86**, 125449 (2012).

[19] Y. H. Wang, H. Steinberg, P. Jarillo-Herrero, and N. Gedik, Observation of Floquet-Bloch states on the surface of a topological insulator, Science **342**, 453 (2013).

[20] N. H. Lindner, G. Refael, and V. Galitski, Floquet topological insulator in semiconductor quantum wells, Nat. Phys. **7**, 490 (2011).

[21] T. Kitagawa, T. Oka, A. Brataas, L. Fu, and E. Demler, Transport properties of nonequilibrium systems under the application of light: Photoinduced quantum Hall insulators without Landau levels, Phys. Rev. B **84**, 235108 (2011).

[22] P. M. Perez-Piskunow, G. Usaj, C. A. Balseiro, and L. E. F. Foa Torres, Floquet chiral edge states in graphene, Phys. Rev. B **89**, 121401 (2014).

[23] M. A. Sentef, M. Claassen, A. F. Kemper, B. Moritz, T. Oka, J. K. Freericks, and T. P. Devereaux, Theory of Floquet band formation and local pseudospin textures in pump-probe photoemission of graphene, Nat. Commun. **6**, 7047 (2015).

[24] J. P. Dahlhaus, B. M. Fregoso, and J. E. Moore, Magnetization signatures of light-induced quantum Hall edge states, arXiv:1408.6811.

[25] A. Quelle, W. Beugeling, and C. M. Smith, Topological Floquet states on a Möbius band irradiated by circularly polarised light, arXiv:1408.3087.

[26] A. López, A. Scholz, B. Santos, and J. Schliemann, Photoinduced pseudospin effects in silicene beyond the off-resonant condition, Phys. Rev. B **91**, 125105 (2015).

[27] N. Goldman and J. Dalibard, Periodically driven quantum systems: Effective Hamiltonians and engineered gauge fields, Phys. Rev. X **4**, 031027 (2014).

[28] S. Choudhury and E. J. Mueller, Stability of a Floquet Bose-Einstein condensate in a one-dimensional optical lattice, Phys. Rev. A **90**, 013621 (2014).

[29] A. Gómez-León, P. Delplace, and G. Platero, Engineering anomalous quantum Hall plateaus and antichiral states with ac fields, Phys. Rev. B **89**, 205408 (2014).

[30] T. Bilitewski and N. R. Cooper, Scattering theory for Floquet-Bloch states, Phys. Rev. A **91**, 033601 (2015).

[31] Y. T. Katan and D. Podolsky, Modulated Floquet topological insulators, Phys. Rev. Lett. **110**, 016802 (2013).

[32] M. S. Rudner, N. H. Lindner, E. Berg, and M. Levin, Anomalous edge states and the bulk-edge correspondence for periodically driven two-dimensional systems, Phys. Rev. X **3**, 031005 (2013).

[33] D. Y. H. Ho and J. Gong, Topological effects in chiral symmetric driven systems, Phys. Rev. B **90**, 195419 (2014).

[34] L. Zhou, H. Wang, D. Y. Ho, and J. Gong, Aspects of Floquet bands and topological phase transitions in a continuously driven superlattice, Eur. Phys. J. B **87**, 204 (2014).

[35] G. Usaj, P. M. Perez-Piskunow, L. E. F. Foa Torres, and C. A. Balseiro, Irradiated graphene as a tunable Floquet topological insulator, Phys. Rev. B **90**, 115423 (2014).

[36] L. D'Alessio and M. Rigol, Dynamical preparation of Floquet Chern insulators: A no-go theorem, the Bott index, and boundary effects, arXiv:1409.6319.

[37] H. Dehghani, T. Oka, and A. Mitra, Dissipative Floquet topological systems, Phys. Rev. B **90**, 195429 (2014).

[38] D. E. Liu, Classification of the Floquet statistical distribution for time-periodic open systems, Phys. Rev. B **91**, 144301 (2015).

[39] K. I. Seetharam, C.-E. Bardyn, N. H. Lindner, M. S. Rudner, and G. Refael, Controlled population of Floquet-Bloch states via coupling to Bose and Fermi baths, arXiv:1502.02664.

[40] T. Iadecola, T. Neupert, and C. Chamon, Occupation of topological Floquet bands in open systems, arXiv:1502.05047.

[41] Z. Gu, H. A. Fertig, D. P. Arovas, and A. Auerbach, Floquet spectrum and transport through an irradiated graphene ribbon, Phys. Rev. Lett. **107**, 216601 (2011).

[42] A. Kundu, H. A. Fertig, and B. Seradjeh, Effective theory of Floquet topological transitions, Phys. Rev. Lett. **113**, 236803 (2014).

[43] L. E. F. Foa Torres, P. M. Perez-Piskunow, C. A. Balseiro, and G. Usaj, Multiterminal conductance of a Floquet topological insulator, Phys. Rev. Lett. **113**, 266801 (2014).

[44] H. Dehghani, T. Oka, and A. Mitra, Out-of-equilibrium electrons and the Hall conductance of a Floquet topological insulator, Phys. Rev. B **91**, 155422 (2015).

[45] N. H. Lindner, D. L. Bergman, G. Refael, and V. Galitski, Topological Floquet spectrum in three dimensions via a two-photon resonance, Phys. Rev. B **87**, 235131 (2013).

[46] Y. Tenenbaum Katan and D. Podolsky, Generation and manipulation of localized modes in Floquet topological insulators, Phys. Rev. B **88**, 224106 (2013).

[47] F. Zhang, C. L. Kane, and E. J. Mele, Surface states of topological insulators, Phys. Rev. B **86**, 081303 (2012).

[48] B. M. Fregoso, Y. H. Wang, N. Gedik, and V. Galitski, Driven electronic states at the surface of a topological insulator, Phys. Rev. B **88**, 155129 (2013).

[49] S. V. Syzranov, M. V. Fistul, and K. B. Efetov, Effect of radiation on transport in graphene, Phys. Rev. B **78**, 045407 (2008).

[50] L. Fu and C. L. Kane, Superconducting proximity effect and majorana fermions at the surface of a topological insulator, Phys. Rev. Lett. **100**, 096407 (2008).

[51] R.-L. Chu, J. Shi, and S.-Q. Shen, Surface edge state and half-quantized Hall conductance in topological insulators, Phys. Rev. B **84**, 085312 (2011).

[52] F. Zhang, C. L. Kane, and E. J. Mele, Surface state magnetization and chiral edge states on topological insulators, Phys. Rev. Lett. **110**, 046404 (2013).

[53] P. M. Perez-Piskunow, L. E. F. Foa Torres, and G. Usaj, Hierarchy of Floquet gaps and edge states for driven honeycomb lattices, Phys. Rev. A **91**, 043625 (2015).

[54] A. J. Niemi and G. W. Semenoff, Axial-anomaly-induced fermion fractionization and effective gauge-theory actions in odd-dimensional space-times, Phys. Rev. Lett. **51**, 2077 (1983).

[55] A. N. Redlich, Parity violation and gauge noninvariance of the effective gauge field action in three dimensions, Phys. Rev. D **29**, 2366 (1984).

[56] X.-L. Qi, T. L. Hughes, and S.-C. Zhang, Topological field theory of time-reversal invariant insulators, Phys. Rev. B **78**, 195424 (2008).

[57] S.-B. Zhang, H.-Z. Lu, and S.-Q. Shen, Edge states and integer quantum Hall effect in topological insulator thin films, arXiv:1502.01792.

[58] Here we exemplify in the truncated basis $m \in \{0,1\}$ for the ZB gap region. For the ZC gap we include the $m = -1$ channel to keep the truncated basis symmetric with respect to the level crossing at $\varepsilon = 0$ [22,35]. The general resolution of the differential equation is, however, completely analogous.

[59] See Supplemental Material at http://link.aps.org/supplemental/10.1103/PhysRevB.91.241404 for more details.

[60] H. Zhang, C.-X. Liu, X.-L. Qi, X. Dai, Z. Fang, and S.-C. Zhang, Topological insulators in Bi_2Se_3, Bi_2Te_3 and Sb_2Te_3 with a single Dirac cone on the surface, Nat. Phys. **5**, 438 (2009).

[61] This was numerically corroborated in a configuration with two laser beams with different frequencies and opposite helicities (see Ref. [59]). Although the time-reversal symmetry is broken everywhere, when continuously connecting the two distinct topological phases the laser-induced band gap necessarily closes at some point in between the two regions [20].